CD24 regulates extracellular vesicle release via an aSMase/PI3K/mTORC2/ROCK/actin pathway in B lymphocytes

Hong-Dien Phan, Willow R.B. Squires, Kaitlyn E. Mayne, Grant R. Kelly, Rashid Jafardoust, Sherri L. Christian*

Department of Biochemistry
Memorial University of Newfoundland
St. John's NL A1C 5S7

*To whom correspondence is to be addressed: sherri.christian@mun.ca

Contact details:
HDP: dhphan@mun.ca, ORCID: 0000-0002-6032-6008
WRBS: willow.squires@mail.utoronto.ca, ORCID: 0000-0002-9433-5148
KEM: kemayne@mun.ca, ORCID: 0009-0002-9481-5819
GRK: gkelly@mun.ca, ORCID: 0009-0003-6986-7454
RJ: rjafardoustb@mun.ca, ORCID: 0000-0002-6636-2667
SLC: sherri.christian@mun.ca, ORCID: 0000-0002-4289-4386

Disclosure Statement: The authors declare no conflicts of interest.

Funding: This work was supported by an NSERC Discovery Grant (RGPIN-2022-03800). HDP was funded by a studentship award supported by MITACS and the Terry Fox Research Institute. WRBS was funded by an Undergraduate Student Research Award from NSERC.

Running Header: Mechanism of ectosome release by CD24

Keywords: CD24, B lymphocyte, extracellular vesicle, ectosome, acid sphingomyelinase (aSMase), ceramide

Word count: 4881

ABSTRACT

CD24 is a glycophosphatidylinositol-linked protein that regulates B cell development. We previously reported that stimulation of CD24 on donor B cells promotes the transport of functional receptors to recipient B cells via extracellular vesicles (EVs). However, the mechanisms regulating EV formation in response to CD24 are unknown. Using bioinformatics, we found a connection between CD24 and the PI3K/AKT and mTOR signaling pathways. To determine if PI3K or mTOR regulates EV release, we made use of our co-culture model, whereby donor B cells carrying the B cell receptor (BCR, IgM) release EVs labeled with palmitoylated GFP upon CD24 stimulation are incubated with recipient B cells that lack IgM and express palmitoylated tdTomato. Using flow cytometry, we are able to follow the transfer of EVs carrying lipid-associated GFP and surface IgM from donor to recipient cells. Using chemical and genetic inhibition, we found that a PI3K/mTORC2/ROCK/actin pathway regulates EV release. We also found that acid sphingomyelinase (aSMase) activates PI3K to induce EV release. Lastly, through live cell imaging, we found that ROCK is required for inducing the membrane dynamics associated with EV release. Overall, our data suggest that these EVs are ectosomes budded from the plasma membrane and not intracellularly-derived exosomes. Importantly, we have uncovered a novel pathway regulating ectosome release.

Introduction

Extracellular vesicles (EVs) are a heterogeneous group of small lipid bilayer-bound particles released by all cells tested to date[1]. There are two primary kinds of EVs described, exosomes and ectosomes, the latter which includes microvesicles, that are distinguished based on their biogenesis[2]. Exosomes originate from intraluminal vesicles (ILVs) that form through the inward budding of the endosomal membrane, resulting in the formation of multivesicular bodies (MVB). This is followed by secretion upon fusion of the MVB with the cell plasma membrane. Exosomes typically range in size from 30 to 150 nm. Exosomes tend to be enriched in a number of proteins including chaperones (Hsp70 and Hsp90), cytoskeletal proteins (actin, myosin, and tubulin), endosomal sorting complex required for transport (ESCRT) proteins (TSG-101 and Alix), proteins involved in transport and fusion (Rab11, Rab7, Rab2, and Annexins), and tetraspanin proteins (CD9, CD63, CD81, and CD82)[2–4]. Ectosomes are generally considered to be 100-1000 nm in diameter and formed by direct outward budding from the surface of the plasma membrane. Ectosomes tend to be enriched in some proteins that differ from exosomes such as GTP-binding protein, ADP-ribosylation factor 6 (ARF6), matrix metalloproteinases (MMPs), glycoproteins (e.g., GPIb, GPIIb-IIIa), integrins, receptors (e.g., EGFRvIII), and cytoskeletal elements (e.g., β-actin and α-actinin-4)[2,3].

Exosome release can be regulated by two distinct processes, namely the ESCRT and ESCRT-independent pathways that also participate in ILV formation. The ESCRTs are made up of four complexes (ESCRT-0, -I, -II, and -III) and the accessory Vps4 complex, each of which is made up of many subunits[5]. The primary job of ESCRT 0-II is to sort cargo on endosomal membranes into functional microdomains. In contrast, Vps4 assists ESCRT-III in completing the process of budding and scission of these domains to produce ILVs[6]. Recent evidence has revealed that TSG101 and ALIX are often seen as exosome constituent proteins and are components of the ESCRT complex. The ESCRT accessory protein ALIX interacts with ESCRT-III subunits to promote intraluminal vesicle budding and abscission[7]. Moreover, Rab GTPases, the most prevalent family of proteins in the Ras superfamily of GTPases, are essential for exosome secretion and play a key role in intracellular vesicle transport, including endosome recycling and MVB trafficking to lysosomes[8]. More research has revealed that many Rab proteins, including Rab27A/B, Rab7, Rab31, and Rab35, are involved in the control of exosome secretion[9]. It has

also been reported that Rab GTPases and SNARE proteins collaborate to cause the release of exosomes into the extracellular space by fusion of late endosomes with the plasma membrane[8,10]. Although the ESCRT pathway is the critical driver of exosome synthesis, other studies have demonstrated exosomes can be released via an ESCRT-independent pathway. For instance, inhibition of the ESCRT-dependent pathway by depleting four ESCRTs did not eliminate MVB formation[11]. Another study reported that the release of exosomes is reduced after inhibition of neutral sphingomyelinase (nSMase), a protein responsible for the production of ceramide, suggesting that the budding of ILVs requires ceramide, an important component of lipid raft microdomains[12]. In addition, ApoE and tetraspanin CD63 are recruited for ILV formation and subsequent exosome release without the requirement of ESCRT or ceramide[13,14].

Ectosome release can be regulated via several pathways. For example, it has been shown that ectosome release can be stimulated through an increase in intracellular Ca^{2+} concentrations[15]. At steady state, the anionic phospholipids, phosphatidylserine (PS) and phosphatidylethanolamine (PE) localize to the inner leaflet of the plasma membrane, while phosphatidylcholine (PC) and sphingomyelin (SM) are found on the external membrane leaflet[16]. The physiological membrane asymmetry is maintained by five transmembrane enzymes: gelsolin, scramblase, flippase, translocase and calpain[17]. The increase in cytoplasmic Ca^{2+} levels inhibits the aminophospholipid translocase and activates lipid scramblase simultaneously[18,19]. This process drives rearrangements in the asymmetry of the membrane phospholipids to expose PS from the inner leaflet to the cell surface. It then leads to the physical collapse of cell membrane asymmetry, which can promote ectosome release[20].

In addition to lipids, cytoskeletal elements and their regulators are required for ectosome formation[21]. Reducing the levels of phosphatidylinositol 4,5-bisphosphate ($PI(4,5)P_2$), which participates in anchoring the membrane to the cortical cytoskeleton, can induce the disruption of the cortical cytoskeleton interaction with the plasma membrane[22,23], leading to increased ectosome biogenesis[24]. Reduction of $PI(4,5)P_2$ can occur via activation of phospholipase C (PLC)-γ, phospholipase D (PLD), phosphoinositide 3-kinases (PI3Ks), or phosphatidylinositol phosphatases[25]. Rab22a and ARF6, members of the Ras GTPase family, also have essential roles in ectosome generation. Rab22A is directly involved in ectosome formation as evidenced by its

colocalization with budding vesicles and the fact that Rab22A knockdown prevents vesicle release[26]. Importantly, ARF6 activity is required for subsequent phospholipase D activation, leading to localized myosin light chain kinase activity at the neck of budding vesicles[27]. Furthermore, ARF6-mediated activation of RhoA and Rho-associated kinase (ROCK) signaling has been implicated in ectosome formation[27,28]. An additional study has shown that the antagonistic interaction between Rab35 and ARF6 also controls ectosome biogenesis[29]. Furthermore, a key regulator in the formation of ectosomes, Ca^{2+} ions also contribute to the reorganization of the cytoskeleton through the activation of cytosolic calpain protease[30]. Calpain cleaves several cytoskeletal components such as actin, ankyrin, protein 4.1 and spectrin[31,32]. Calpain-mediated cleavage of the cytoskeleton further disrupts the cortical cytoskeleton protein network, consequently, allowing membrane budding[33]. Lastly, similar to exosomes, ceramide production can increase ectosome release[34].

CD24 (also known as heat stable antigen) is a glycophosphatidylinositol (GPI)-anchored glycoprotein, which is localized to lipid rafts on the plasma membrane[35]. It contains 27 amino acids with extensive N-linked and O-linked glycosylation that can result in variable molecular weight products. CD24 is expressed on several cell types, including B cells, T cells, neutrophils, eosinophils, dendritic cells, macrophages, epithelial cells, and cancer cells. During B cell development in the bone marrow, CD24 is first expressed by pro-B cells (also called Fraction B) but is also highly expressed at the pre-B cell (Fraction C, C’, and D) stages and in transitional B cells[36].

One of the most well-described effects of CD24-mediated signaling is its promotion of apoptosis in developing B cells[37]. CD24 recruits Src family protein tyrosine kinases (PTKs) to activate signalling pathways via direct protein phosphorylation, intracellular calcium mobilization, and transcription factor activation[36]. Moreover, existing evidence has demonstrated that multiple cancer related signaling pathways, such as Wnt/b-catenin, mitogen activated protein kinase (MAPK), Src or PI3K/Akt, Notch, and Hedgehog, are activated downstream of CD24[38].

We previously discovered that the engagement of CD24 enhances the release of EVs from *ex vivo* bone marrow-derived B cells and the mouse WEHI-231 B cell lymphoma cell lines[39]. We

also found that the RNA cargo and the EV proteome are relatively stable, but the composition of the membrane proteins on the EVs is altered[40]. Recently, we employed a model system where donor cells expressing palmitoylated GFP (WEHI-231-GFP cells) were co-cultured, after CD24 stimulation, with recipient cells lacking IgM and expressing palmitoylated tdTomato (WEHI-303-tdTomato cells) to study EV-mediated transfer of functional receptors. We found that EVs trafficked lipid and membrane proteins between B lymphocytes in response to stimulation of CD24 on the donor cells. Notably, the transported receptors can induce apoptosis, which may affect B cell development in recipient bystander B cells during B cell development[41]. The data from our previous studies suggest that the EVs induced by CD24 stimulation are ectosomes budded off the plasma membrane, not exosomes derived from MVBs. However, the underlying mechanisms that govern ectosome formation in response to engagement of CD24 have not been described.

We first analyzed the expression of genes differentially expressed in the same manner as CD24 across B cell development using a dataset from the Immunological Genome Project (ImmGen) database[42]. Network analysis revealed that CD24 expression is associated with genes that are enriched in the PI3K/Akt/mTOR signaling pathway. Therefore, in this study, we addressed the hypothesis that CD24-mediated ectosome release is regulated by the PI3K/Akt/mTOR pathway. Using our co-culture model, we found that CD24 mediates ectosome release via the activation of acid sphingomyelinase (aSMase), which activates the PI3K/mTORC2/ROCK pathways followed by actin cytoskeletal rearrangement.

Materials and Methods

Cell culture

WEHI-231 cells (American Type Culture Collection (ATCC), Manassas, VA) and WEHI-303.1.5 (WEHI-303)[43] were transfected with a lentiviral plasmid encoding either palm-GFP (WEHI-231-GFP) or palm-tdTomato (WEHI-303-tdTomato) obtained from Charles Lai, Institute of Atomic and Molecular Sciences, Taiwan[44]. Cells were cultured in RPMI-1640 medium (Gibco) containing 10% heat□inactivated fetal bovine serum (FBS) (Gibco), 1.0 mM sodium pyruvate (Gibco), 50 mM 2-mercaptoethanol (Sigma) and 100 U/ml penicillin, 100 µg/ml streptomycin (Invitrogen). For knockdown experiments, WEHI-231-GFP cells (2×10^5) were transiently

transfected with 2 mM siRNA with the Neon Transfection Kit (MPK1025B, Invitrogen) using the Neon Electroporation system according to the manufacturer's instructions. The siRNAs used were control non-targeting siRNA-A (Santa Cruz Biotechnology, SC-37007), PI 3-kinase p110δ siRNA (Santa Cruz Biotechnology, SC-39132), and Rock-1 siRNA (Santa Cruz Biotechnology, SC-36432). Cells were pulsed once with a voltage of 1700 and a width of 20. Transfected cells were cultured for 55 h before use.

Bioinformatics

ImmGen data (accession number GSE15907), containing gene expression data for B cells in the Fraction (Fr) A-F stages of development, was identified. The microarray gene expression data files for Fr A, Fr B/C, Fr C', Fr D, and Fr F were background corrected and robust multi-array average (RMA) normalized using the Oligo, Biobase, and pd.mogene.1.0.st.v1 Bioconductor packages in R version 4.0.0. A list of differentially expressed genes with similar expression patterns to *Cd24a* was then compiled using the Limma and Affycoretools Bioconductor packages. Fr A B cells (pre-pro B cells) was used as the negative control for the differential expression analysis.

Differential expression analysis produced a list of 1838 genes expressed in a similar manner as *Cd24a*. The gene transcript cluster ID list was annotated with the corresponding gene names using the NetAffx analysis batch query and merged with the R expression data to create a median linkage hierarchical cluster in Genesis version 1.8.1. A clade of 44 genes whose expression patterns were most similar to that of *Cd24a* was identified (Figure 1A). Of the 44 genes in the clade, 41 were annotated. These 41 genes were used to generate pathway networks in Cytoscape version 3.8.0 using the ClueGO plugin version 2.5.7. The analysis used pathway network data from the KEGG, REACTOME Pathways, and WikiPathways databases to compile a network of signaling pathways associated with the 41 gene list.

Phosphatidylinositol (3,4,5)-trisphosphate (PIP_3) Quantification

WEHI-231-GFP cells (0.5×10^6) were pre-treated for 15 min with the PI3K inhibitor, 10μM LY294002 (9901, Cell Signaling Technology), 10 μM imipramine (J63723.06, Alfa Aesar), or with an equal volume of DMSO. Cells were then stimulated with 10 μg/ml of functional grade

primary monoclonal M1/69 rat anti-mouse CD24 antibody (16-0242085, eBioscience) or 10 µg/ml matching primary isotype antibody (16-4031-85, eBioscience) that was pre-incubated with 5 µg/ml goat anti-rat secondary antibody (112-005-003, Jackson ImmunoResearch) for 15 min. After treatment, cells were centrifuged and phosphoinositides were extracted and measured using the PIP_3 ELISA kit (Creative Diagnostic, DEIA-XYZ6). All experiments were performed at least four times, each carried out in duplicate according to the manufacturer's instructions.

Analysis of cell surface IgM and lipid transfer by flow cytometry

WEHI-231-GFP cells (0.5 x 10^6) were pre-treated with either DMSO or inhibitor for 15 min. The following inhibitors were used: 10 µM LY294002, 0.25 µM MK2206 (S1078, Selleckchem), 0.25 µM Torin 1 (14379S, Cell Signaling Technology), 0.1 µM Rapamycin (A8167, APExBIO), 0.1 µM JR-AB2-011 (HY-122022, MedChemExpress), 10 µM Y27632 (13624S, Cell Signaling Technology), 0.2 µM Cytochalasin D (PHZ1063, Gibco, ThermoFisher), 10 µM imipramine, 20 µM GW4869 (D1692, Sigma Aldrich), or 0.5 µg/mL Ionomycin (I24222, Thermo Fisher). Cells were stimulated with anti-mouse CD24 antibody or isotype antibody as above followed by centrifugation to remove excess antibody. Cells were then co-cultured with the recipient WEHI-303-tdTomato cells (0.5 x 10^6) for 24 h. To assess cell surface IgM and lipid transfer, the mixed cells were resuspended in ice-cold FACS buffer (1x PBS, pH 7.4, containing 1% heat-inactivated FBS) and then stained on ice for 30 min with 0.5 mg of IgM-PE-Cy7 (25-5890, eBioscience) to detect IgM. Cells were then washed with FACS buffer and analyzed by flow cytometry. Flow cytometry was performed using a CytoFLEX (Beckman Coulter) counting at least 10,000 events and data were analyzed using FlowJo software version 10.4.1.

Immunoblotting

Cell extracts were separated on 8% to 15% SDS-PAGE gels and transferred to nitrocellulose membranes, which were blocked with either 5% milk powder or 5% BSA in 0.1% Tween-20-Tris-buffered saline (TBST) for 1 h at room temperature. The membranes were incubated with primary antibody in TBST overnight at 4°C: Phospho-Akt (Ser473) antibody (Cell Signaling Technology, #9271, 1:1000), Akt (Cell Signaling Technology, #9272, 1:1000), Phospho-cofilin (Cell Signaling Technology, #3313; 1:1000), cofilin (Cell Signaling Technology, #3318, 1:1000), Rock-1 antibody (G-6) (Santa Cruz Biotechnology, SC-17794, 1:500), PI3K p110δ antibody (A-

8) (Santa Cruz Biotechnology, SC-55589, 1:1000), GAPDH (G-9) (Santa Cruz Biotechnology, SC-365062, 1:1000). The membrane was washed and incubated with a horseradish peroxidase (HRP)-conjugated goat anti-rabbit IgG (H+L) (Bio Rad, #1706515) or goat anti-mouse IgG (H+L) (Bio Rad, #1721011). Immunoreactive bands were visualized on a Chemidoc gel system (BioRad) using an ECL substrate (WBULS0100, Millipore). Image manipulation involved adjustments to brightness and contrast only.

Live cell imaging

35 mm glass coverslips were cleaned thrice with 1x PBS and incubated with 1 mg/mL of anti-MHC class II antibody (Sigma, MABF33) overnight at 4°C. Then, 0.5 x 10^6 WEHI-231-GFP cells were seeded onto the glass coverslips for 30 min at 4°C. The cells were washed with PBS and visualized with a Carl Zeiss LSM 880 laser scanning microscope system with a 63x oil immersion lens with numerical aperture (NA) of 1.4 objective under environment at 37°C and 5% CO_2. Laser excitation light was provided at a wavelength of 488 nm, and fluorescent emissions were collected at wavelengths above 515 nm. For image acquisition, an exposure time of 0.8 second was adopted with a binning of 2 x 2 yielding a pixel size of 0.68 mm. Individual cells within a single field of view were captured with an Airyscan detector over a 5-min period for 250 cycles, with a 1.2-second shuttered interval between each image. Raw Airyscan images were processed using the Zeiss Zen Blue analysis software. Subsequent image processing was conducted in ImageJ to create a video with 25 frames per second for a 10-second length.

Statistical analysis

One-way ANOVA and two-way ANOVA with Sidak's post-hoc test were performed using GraphPad Prism (version 10.1.1) software, as indicated.

Results

Prior research from our lab showed that B cells release EVs in response to CD24 engagement[39–41]. As the first step in attempting to elucidate the pathway(s) responsible for CD24-mediated release of EVs, we performed a bioinformatics-based analysis to find potential signaling pathways linked to CD24 expression in developing B cells. We identified 44 genes in the clade

that that most closely resembled *Cd24a* (Figure 1A). Of these, 41 could be used to predict CD24-related signaling pathways. In the networks of connected pathway terms, seven of the nodes had terms related to PI3K/Akt/mTOR signalling (Figure 1B). Thus, we predicted that CD24 may activate PI3K signaling. To determine if engagement of CD24 activated PI3K, we analyzed the levels of PIP_3, the immediate product of PI3K activation. We found that PIP_3 levels were significantly increased in response to CD24 stimulation, but not with isotype-control stimulated cells. In addition, we observed the increase of PIP_3 was inhibited in the presence of the PI3K inhibitor, LY294002 (LY, Figure 1C). These results clearly demonstrate that CD24 triggers B cells to activate PI3K.

To determine if the PI3K signaling pathway regulates EV release in response to CD24 stimulation, we used our model system to track EV transfer (Supplemental Figure 1A-C). Transfer of EVs, as shown previously[41], can be evaluated by the uptake of GFP and IgM in the recipient tdTomato-positive cells. We found a significant increase in lipid transfer between the CD24-stimulated and the isotype-stimulated group in either the absence or presence of the inhibitor. However, the amount of lipid transferred in response to CD24 was significantly reduced in the presence of LY (Figure 2A and Supplemental Figure 1D). Parallel investigations into protein transfer revealed a similar pattern. There was a significant increase in protein transfer between the CD24-stimulated and the isotype-stimulated group in the presence or absence of LY with significantly less transfer in the CD24-stimulated group in the presence of LY (Figure 2B and Supplemental Figure 1E). To verify inhibition of the PI3K pathway, we analyzed Akt phosphorylation. We found that the level of phosphorylated AKT increased in response to CD24 stimulation, while it was markedly lower in cells pre-treated with LY compared with those that received DMSO (Figure 2C). Thus, these data show that LY inhibits CD24-mediated PI3K signaling; however, some residual activation remains.

Next, we sought to genetically validate the LY result using siRNA knock-down of PI3K in donor cells. The absence of PI3K expression in siRNA-transfected WEHI-231-GFP cells was confirmed by Western blot (Figure 2D). Analysis of lipid and protein transfer between the CD24-stimulated and isotype-stimulated groups revealed a significant increase in the scrambled control siRNA group, as expected. However, there was no transfer of lipid or protein in either the

isotype-stimulated or CD24-stimulated groups when PI3K was knocked-down in the donor cells (Figure 2E-F). These findings strongly support a role for the PI3K signaling pathway in regulating CD24-mediated EV production.

We investigated further to see if proteins downstream of PI3K are involved in EV release in response to CD24. Akt is an important downstream kinase of PI3K, and it can be activated in response to phosphorylation by PI3K-mediated activation of the PDK1 and mTORC2 kinases[45,46]. Phosphorylated Akt can activate multiple downstream signaling molecules, including TSC2, GSK3, and BAD, which drive cell growth, survival, and angiogenesis[47]. After pre-treatment with the Akt inhibitor MK-2206, we found a significant decrease in CD24-mediated lipid and protein transfer to recipient cells (Figure 3A-B). Similar to PI3K inhibition, some residual EV transfer remained in the presence of the inhibitor.

Other signalling pathways downstream of PI3K are the mTOR signalling pathways. mTOR forms two structurally and functionally distinct complexes called mTORC1 and mTORC2[48]. Therefore, we next determined if mTORC1 or mTORC2 regulates CD24-mediated EV release. To do this, we used Torin 1, an inhibitor of mTORC1/2, rapamycin, an inhibitor of mTORC1, and JR-AB2-011, an inhibitor of mTORC2[49]. As can be seen in Figure 3C and Figure 3D, there was a substantial statistical difference in lipid and protein transfer between the mTORC2 inhibition groups (Torin 1 and JR-AB2-011) and the control stimulated group, indicating that mTORC2 controls EV release in response to CD24.

Rho-associated protein kinase (ROCK) is known to be regulated by the PI3K/mTORC2 signaling pathway[50] and was identified by the bioinformatics analysis (Figure 1B). Therefore, we next asked whether CD24-mediated EV release was similarly regulated by the ROCK signaling pathway using the inhibitor Y27632[51]. We found that, in comparison to EVs from the control group, the release of EVs from donor cells pre-treated with Y27632 resulted in a significantly lower transfer of lipid and protein to recipient cells upon CD24 stimulation (Figure 4A-B). We found that there was a reduction but not a total block in phosphorylated cofilin, a downstream target of ROCK, suggesting that the inhibitor did not fully block ROCK activity (Figure 4C). Next, to genetically validate the Y27632 inhibitor result, we used siRNA to knock-down ROCK

in donor cells (Figure 4D). We found that there was no transfer of lipids or proteins with CD24 stimulation when ROCK was knocked-down (Figure 4E-F). These data clearly demonstrate that CD24-mediated EV generation is regulated by ROCK.

We hypothesized that dynamic cytoskeletal reorganization downstream of ROCK that changes the shape of cell membrane will, in turn, promote EV release. Donor cells were thus pre-treated with cytochalasin D to prevent cytoskeleton rearrangement. The results showed that there was no increase in lipid and protein transfer in the cytochalasin D-treated CD24-stimulated group compared to the control stimulation (Figure 5A-B). Thus, actin cytoskeleton regulation plays a key role in regulating CD24-mediated EV release.

Sphingomyelin (SM), a phospholipid that localizes on the plasma membrane's outer leaflet and has a strong affinity for cholesterol, plays a significant role in determining the fluidity and structural integrity of the plasma membrane[52]. nSMase and aSMase catalyze the hydrolysis of SM to ceramide, a process that is involved in both exosome and ectosome release[53]. Exosome release has been previously shown to be regulated by nSMase, which can be blocked by GW4869[12], while a previous study has shown that imipramine blocked ectosome formation from glial cells by inhibiting aSMase[34]. Thus, we treated donor cells with either GW4869 or imipramine to determine if nSMase or aSMase regulates CD24-mediated EV release. We found that there was no difference in lipid and protein transfer with GW4896 (Supplemental Figure 2A-B). In contrast, CD24-mediated lipid and protein transfer were significantly inhibited with imipramine treatment (Figure 5C-D). These findings show that aSMase, but not nSMase, regulates CD24-mediated EV release. These data are consistent with our previous studies that suggested that the EVs induced by CD24 stimulation are ectosomes budded off the plasma membrane and not exosomes derived from MVBs[39–41].

We next determined if PI3K was upstream or downstream of aSMase by determining if inhibition of aSMase alters PIP_3 levels in response to CD24 stimulation. We found that the CD24-mediated increase of PIP_3 was significantly inhibited in the presence of imipramine (Figure 5E). Therefore, aSMase activation is upstream of PI3K.

Although we successfully determined that inhibiting EV release from CD24-mediated B cells is via an aSMase, PI3K, and ROCK, we wanted to determine if these are all in the same pathway by simultaneously inhibiting two pathways. Lipid transfer was completely blocked by both single and double inhibitor treatments (Figure 6A). However, there remained residual protein transfer in both the single and double inhibitor pre-treatments, which was not significantly different (i.e. the inhibitors were not additive) (Figure 6B). Therefore, these data suggest that aSMase/PI3K/ROCK are all in the same pathway.

Lastly, we performed live cell imaging to visualize EV release and membrane dynamics. We clearly saw the plasma membrane labeled with GFP, which displayed a substantial increase in dynamic movement when cells were stimulated through CD24 (Figure 7A and Supplemental Video Files 1-8). In some cases, we were able to visualize EV-like structures budding from the plasma membrane with more of these structures visible in CD24-stimulated cells; however, this was extremely difficult to quantify as the structures were very transient. We observed a reduction in membrane dynamics in the presence of PI3K and ROCK inhibitors during CD24 treatment when highly active cells were counted; however, only ROCK inhibition had a statistically significant effect (Figure 7B-C). These data suggest that the induction of membrane dynamics necessary for EV release requires ROCK activation.

Discussion

We have identified a novel pathway regulating ectosome release, namely aSMase/PI3K/mTORC2/ROCK/actin pathway. By exploiting bioinformatics pathway analysis, we were able to identify PI3K and mTOR as potential nodes regulating CD24-mediated EV release. Further elucidation of potential regulators allowed us to determine that this pathway is initiated by aSMase which, through an unknown mechanism, activates PI3K to promote actin rearrangement downstream of the mTORC2/ROCK axis. To the best of our knowledge, this is the first time that CD24 has been linked to PI3K and to aSMase. In addition, this is the first report of PI3K regulating ectosome release. One previous publication linked PI3K to the

generation of ABCG2-rich EVs in breast cancer cells; however, these EVs were most likely exosomes[54].

This study revealed a range of pharmacological agents that can effectively inhibit the release of ectosomes. The first inhibitor, LY294002, is an inhibitor of PI3K. Generation of PIP_3 from $PI(4,5)P_2$ by PI3K recruits protein kinase B (Akt), phosphoinositide-dependent kinase 1 (PDK1), and mTORC2 resulting in their colocalization. This permits PDK1 to phosphorylate Akt on threonine 308 and mTORC2 to phosphorylate serine 473[45,46]. The second inhibitor, MK2206, is an inhibitor of Akt. PI3K/Akt signaling is implicated in various cellular processes, including differentiation, growth, proliferation, and intracellular trafficking, all of which are factors in B cell development and activation[45,46]. mTOR is found in two complexes: mTORC1 (which contains mTOR, Raptor, and other proteins) and mTORC2 (which contains mTOR, Rictor, and other proteins)[55]. mTORC1, called the rapamycin-sensitive mTOR complex, is a key regulator of cell proliferation and survival downstream of the PI3K/Akt pathway. It activates protein synthesis through modulation of the 40S ribosomal protein S6 kinase and the translational initiation factor elF-4E binding protein 1[56]. In contrast, the rapamycin-insensitive, rictor-containing complex (mTORC2) is assembled via binding of PIP_3 by the PH-domain containing protein mSIN1, and thereby relieving its suppression on mTOR kinase activity[57]. As mentioned, mTORC2 triggers Akt activation by phosphorylation on serine 473, as well as regulation of the actin cytoskeleton via RhoA and PKCα[58]. We used Torin1, rapamycin and JR-AB2-011 to determine if mTORC1 or mTORC2 is involved in the release of EVs. We found that mTORC2, but not mTORC1, is essential for CD24-mediated EV release. The sixth inhibitor, Y27632, is an inhibitor of RhoA. ROCK is a downstream effector of RhoA, which exists in two isoforms, ROCK1 and ROCK2. The Rho/ROCK signalling system is involved in multiple cellular processes such as cell growth, differentiation, and cytoskeleton regulation[59]. The seventh inhibitor tested, cytochalasin D, disrupts actin filaments of the cytoskeleton, particularly inhibiting actin polymerization. In addition, we provide evidence, by live cell imaging, that ROCK signaling regulates EV release in response to CD24 stimulation, likely by regulating actin anchorage to the plasma membrane. In addition, increases in PIP_3 can also regulate anchorage of the actin cytoskeleton by reducing the available $PI(4,5)P_2$[22,23]. These findings expand our

understanding of the molecular mechanisms governing CD24-mediated EV release and highlights the complexity of the signaling networks underlying this process.

Contrary to the previous report[15,33], we did not find any involvement of intracellular calcium in the regulation of ectosome release (Supplemental Figure 2B).

Lipid rafts play a key role in the synthesis and function of EVs[60]. Ceramide-enriched lipid rafts have also been found in exosomal membranes[61]. Herein, we report decreased levels of EV transfer in the presence of imipramine, which prevents the activation of aSMase, and the subsequent increase in ceramide levels. Thus, in these cells, aSMase is likely inducing the formation of ceramide-enriched lipid rafts, which in turn promotes the membrane curvature needed for EV formation[62]. The increase in local ceramide concentrations might displace cholesterol in the lipid rafts to alter their function and initiate signal transduction[63]. However, alterations in lipid composition in lipid rafts in response to CD24 stimulation has yet to be determined.

Previous work has linked CD24 to the recruitment of PTEN, a negative regulator of PI3K signaling, to the plasma membrane to induce autophagy by inhibition of downstream proteins Akt and mTORC1[64]. However, this is opposite to what we found, which was an activation of PI3K by CD24. CD24 has been found to mediate signal transduction by recruiting Src family protein tyrosine kinases, including Fgr, Lyn, and Lck to lipid rafts[37,38]. Specifically, Lyn is activated by CD24 in B cells[37]. Lyn activates PI3K in colorectal cancer cells and myeloma cells[65,66]. In endometrial cells, Lyn has been shown to be activated by long chain glucosylceramide and in neutrophils by lactosylceramide[67,68]. Therefore, activation of Lyn by re-organization of lipid raft components due to the increase in ceramide, as discussed above, may promote the activation of PI3K downstream of CD24.

Sphingolipids are an essential class of bioactive lipids. Ceramide is the principal sphingolipid metabolite that is produced through three main synthesis pathways, including the *de novo* pathway in the endoplasmic reticulum, the salvage pathway in the lysosome, and sphingomyelinase (SMase) both in lysosome and plasma membranes[69]. There are three types of

SMase: nSMase, aSMase, and alkaline SMase named based on their pH optima[70]. aSMase is further divided into lysomal and secreted forms. Secretory aSMase translocates onto the cell surface from intracellular vesicles[71]. At the outer leaflet of the plasma membrane, aSMase hydrolyzes sphingomyelin into ceramide[72], generating ceramide-enriched lipid rafts that induce membrane curvature[73] and facilitate membrane blebbing and shedding[53]. It was reported that aSMase and ceramide are involved in ectosome release from glial cells, which requires p38 MAPK activation[34]. Our findings that aSMase, and not nSMase, induces EV release supports our earlier research suggesting that the EVs generated by CD24 stimulation are not exosomes derived from multivesicular bodies, but rather ectosomes that have budded off the plasma membrane[39–41]. Future work will be needed to understand the mechanism that regulates CD24 activation of aSMase.

In sphingolipid metabolism, ceramide can be broken down by ceramidases to produce sphingosine[74]. Ceramide and sphingosine both work by activating PKCδ and protein phosphatase 2A to suppress Akt activity, thereby inducing cell cycle arrest and promoting apoptosis[47]. On the other hand, ceramide can be metabolized to ceramide-1-phosphate (C1P) by ceramide kinase. C1P can be converted back to ceramide by lipid phosphate phosphatases[75]. Alternatively, sphingosine can be phosphorylated by sphingosine kinase to produce sphingosine-1-phosphate (S1P)[75]. It is reported that both C1P and S1P activate PI3K, consequently contributing to cell survival and cell proliferation[76–78]. However, the appropriate balance between the amounts of these two metabolites for cell and tissue homeostasis is unknown. Here, we show that aSMase activates PI3K. However, whether this activation is via increases in ceramide or C1P levels has yet to be determined.

In summary, here we provide compelling evidence that CD24 activates an aSMase/PI3K/mTORC2/ROCK/actin signaling pathway to induce ectosome formation. Importantly, these findings provide a new avenue for research into the regulation of ectosome generation.

References

1. Buzas, E. I. The roles of extracellular vesicles in the immune system. *Nat. Rev. Immunol.* **23**, 236–250 (2023).
2. van Niel, G., D'Angelo, G. & Raposo, G. Shedding light on the cell biology of extracellular vesicles. *Nat. Rev. Mol. Cell Biol.* **19**, 213–228 (2018).
3. Maas, S. L. N., Breakefield, X. O. & Weaver, A. M. Extracellular Vesicles: Unique Intercellular Delivery Vehicles. *Trends Cell Biol.* **27**, 172–188 (2017).
4. Colombo, M. *et al.* Analysis of ESCRT functions in exosome biogenesis, composition and secretion highlights the heterogeneity of extracellular vesicles. *J. Cell Sci.* **126**, 5553–5565 (2013).
5. Henne, W. M., Buchkovich, N. J. & Emr, S. D. The ESCRT Pathway. *Dev. Cell* **21**, 77–91 (2011).
6. Henne, W. M., Stenmark, H. & Emr, S. D. Molecular Mechanisms of the Membrane Sculpting ESCRT Pathway. *Cold Spring Harb. Perspect. Biol.* **5**, a016766 (2013).
7. Zhang, Y., Liu, Y., Liu, H. & Tang, W. H. Exosomes: biogenesis, biologic function and clinical potential. *Cell Biosci.* **9**, 19 (2019).
8. Blanc, L. & Vidal, M. New insights into the function of Rab GTPases in the context of exosomal secretion. *Small GTPases* **9**, 95–106 (2017).
9. Jin, Y. *et al.* Extracellular signals regulate the biogenesis of extracellular vesicles. *Biol. Res.* **55**, 35 (2022).
10. Liu, C. *et al.* Identification of the SNARE complex that mediates the fusion of multivesicular bodies with the plasma membrane in exosome secretion. *J. Extracell. Vesicles* **12**, 12356 (2023).

11. Stuffers, S., Sem Wegner, C., Stenmark, H. & Brech, A. Multivesicular endosome biogenesis in the absence of ESCRTs. *Traffic Cph. Den.* **10**, 925–937 (2009).
12. Trajkovic, K. *et al*. Ceramide triggers budding of exosome vesicles into multivesicular endosomes. *Science* **319**, 1244–1247 (2008).
13. van Niel, G. *et al*. Apolipoprotein E Regulates Amyloid Formation within Endosomes of Pigment Cells. *Cell Rep.* **13**, 43–51 (2015).
14. van Niel, G. *et al*. The tetraspanin CD63 regulates ESCRT-independent and dependent endosomal sorting during melanogenesis. *Dev. Cell* **21**, 708–721 (2011).
15. Bucki, R., Bachelot-Loza, C., Zachowski, A., Giraud, F. & Sulpice, J. C. Calcium induces phospholipid redistribution and microvesicle release in human erythrocyte membranes by independent pathways. *Biochemistry* **37**, 15383–15391 (1998).
16. Bretscher, M. S. Asymmetrical lipid bilayer structure for biological membranes. *Nature. New Biol.* **236**, 11–12 (1972).
17. Piccin, A., Murphy, W. G. & Smith, O. P. Circulating microparticles: pathophysiology and clinical implications. *Blood Rev.* **21**, 157–171 (2007).
18. Comfurius, P. *et al*. Loss of membrane phospholipid asymmetry in platelets and red cells may be associated with calcium-induced shedding of plasma membrane and inhibition of aminophospholipid translocase. *Biochim. Biophys. Acta BBA - Biomembr.* **1026**, 153–160 (1990).
19. Hankins, H. M., Baldridge, R. D., Xu, P. & Graham, T. R. Role of flippases, scramblases, and transfer proteins in phosphatidylserine subcellular distribution. *Traffic Cph. Den.* **16**, 35–47 (2015).

20. Gonzalez, L. J. *et al.* The influence of membrane physical properties on microvesicle release in human erythrocytes. *PMC Biophys.* **2**, 7 (2009).

21. Pap, E., Pállinger, E., Pásztói, M. & Falus, A. Highlights of a new type of intercellular communication: microvesicle-based information transfer. *Inflamm. Res. Off. J. Eur. Histamine Res. Soc. Al* **58**, 1–8 (2009).

22. Raucher, D. *et al.* Phosphatidylinositol 4,5-Bisphosphate Functions as a Second Messenger that Regulates Cytoskeleton–Plasma Membrane Adhesion. *Cell* **100**, 221–228 (2000).

23. Niebuhr, K. *et al.* Conversion of PtdIns(4,5)P2 into PtdIns(5)P by the S.flexneri effector IpgD reorganizes host cell morphology. *EMBO J.* **21**, 5069–5078 (2002).

24. Flaumenhaft, R. Formation and fate of platelet microparticles. *Blood Cells. Mol. Dis.* **36**, 182–187 (2006).

25. Nebl, T., Oh, S. W. & Luna, E. J. Membrane cytoskeleton: PIP2 pulls the strings. *Curr. Biol.* **10**, R351–R354 (2000).

26. Wang, T. *et al.* Hypoxia-inducible factors and RAB22A mediate formation of microvesicles that stimulate breast cancer invasion and metastasis. *Proc. Natl. Acad. Sci. U. S. A.* **111**, E3234–E3242 (2014).

27. Muralidharan-Chari, V. *et al.* ARF6-regulated shedding of tumor cell-derived plasma membrane microvesicles. *Curr. Biol. CB* **19**, 1875–1885 (2009).

28. Sedgwick, A. E., Clancy, J. W., Olivia Balmert, M. & D'Souza-Schorey, C. Extracellular microvesicles and invadopodia mediate non-overlapping modes of tumor cell invasion. *Sci. Rep.* **5**, 14748 (2015).

29. Li, B., Antonyak, M. A., Zhang, J. & Cerione, R. A. RhoA triggers a specific signaling pathway that generates transforming microvesicles in cancer cells. *Oncogene* **31**, 4740–4749 (2012).

30. Taylor, J., Azimi, I., Monteith, G. & Bebawy, M. Ca2+ mediates extracellular vesicle biogenesis through alternate pathways in malignancy. *J. Extracell. Vesicles* **9**, 1734326 (2020).

31. Perrin, B. J., Amann, K. J. & Huttenlocher, A. Proteolysis of cortactin by calpain regulates membrane protrusion during cell migration. *Mol. Biol. Cell* **17**, 239–250 (2006).

32. Storr, S. J., Carragher, N. O., Frame, M. C., Parr, T. & Martin, S. G. The calpain system and cancer. *Nat. Rev. Cancer* **11**, 364–374 (2011).

33. Roseblade, A., Luk, F., Ung, A. & Bebawy, M. Targeting microparticle biogenesis: a novel approach to the circumvention of cancer multidrug resistance. *Curr. Cancer Drug Targets* **15**, 205–214 (2015).

34. Bianco, F. *et al.* Acid sphingomyelinase activity triggers microparticle release from glial cells. *EMBO J.* **28**, 1043–1054 (2009).

35. Kay, R., Rosten, P. M. & Humphries, R. K. CD24, a signal transducer modulating B cell activation responses, is a very short peptide with a glycosyl phosphatidylinositol membrane anchor. *J. Immunol. Baltim. Md 1950* **147**, 1412–1416 (1991).

36. Fang, X., Zheng, P., Tang, J. & Liu, Y. CD24: from A to Z. *Cell. Mol. Immunol.* **7**, 100–103 (2010).

37. Suzuki, T. *et al.* CD24 Induces Apoptosis in Human B Cells Via the Glycolipid-Enriched Membrane Domains/Rafts-Mediated Signaling System1. *J. Immunol.* **166**, 5567–5577 (2001).

38. Yang, Y., Zhu, G., Yang, L. & Yang, Y. Targeting CD24 as a novel immunotherapy for solid cancers. *Cell Commun. Signal.* **21**, 312 (2023).

39. Ayre, D. C. *et al.* Dynamic regulation of CD24 expression and release of CD24-containing microvesicles in immature B cells in response to CD24 engagement. *Immunology* **146**, 217–233 (2015).

40. Ayre, D. C. *et al.* CD24 induces changes to the surface receptors of B cell microvesicles with variable effects on their RNA and protein cargo. *Sci. Rep.* **7**, 8642 (2017).

41. Phan, H.-D. *et al.* CD24 and IgM Stimulation of B Cells Triggers Transfer of Functional B Cell Receptor to B Cell Recipients Via Extracellular Vesicles. *J. Immunol. Baltim. Md 1950* **207**, 3004–3015 (2021).

42. Heng, T. S. P. *et al.* The Immunological Genome Project: networks of gene expression in immune cells. *Nat. Immunol.* **9**, 1091–1094 (2008).

43. Page, D. M., Gold, M. R., Fahey, K. A., Matsuuchi, L. & DeFranco, A. L. Mutational analysis of antigen receptor regulation of B lymphocyte growth. Evidence for involvement of the phosphoinositide signaling pathway. *J. Biol. Chem.* **266**, 5563–5574 (1991).

44. Lai, C. P. *et al.* Visualization and tracking of tumour extracellular vesicle delivery and RNA translation using multiplexed reporters. *Nat. Commun.* **6**, 7029 (2015).

45. Jellusova, J. & Rickert, R. C. The PI3K Pathway in B Cell Metabolism. *Crit. Rev. Biochem. Mol. Biol.* **51**, 359–378 (2016).

46. Limon, J. J. & Fruman, D. A. Akt and mTOR in B Cell Activation and Differentiation. *Front. Immunol.* **3**, 1–12 (2012).

47. Yu, L., Wei, J. & Liu, P. Attacking the PI3K/Akt/mTOR signaling pathway for targeted therapeutic treatment in human cancer. *Semin. Cancer Biol.* **85**, 69–94 (2022).

48. Panwar, V. *et al*. Multifaceted role of mTOR (mammalian target of rapamycin) signaling pathway in human health and disease. *Signal Transduct. Target. Ther.* **8**, 1–25 (2023).
49. Zhou, H., Luo, Y. & Huang, S. Updates of mTOR inhibitors. *Anticancer Agents Med. Chem.* **10**, 571–581 (2010).
50. Dai, H. & Thomson, A. W. The "other" mTOR complex: new insights into mTORC2 immunobiology and their implications. *Am. J. Transplant. Off. J. Am. Soc. Transplant. Am. Soc. Transpl. Surg.* **19**, 1614–1621 (2019).
51. Catalano, M. & O'Driscoll, L. Inhibiting extracellular vesicles formation and release: a review of EV inhibitors. *J. Extracell. Vesicles* **9**, 1703244 (2020).
52. Simons, K. & Ikonen, E. Functional rafts in cell membranes. *Nature* **387**, 569–572 (1997).
53. Verderio, C., Gabrielli, M. & Giussani, P. Role of sphingolipids in the biogenesis and biological activity of extracellular vesicles. *J. Lipid Res.* **59**, 1325–1340 (2018).
54. Goler-Baron, V., Sladkevich, I. & Assaraf, Y. G. Inhibition of the PI3K-Akt signaling pathway disrupts ABCG2-rich extracellular vesicles and overcomes multidrug resistance in breast cancer cells. *Biochem. Pharmacol.* **83**, 1340–1348 (2012).
55. Guertin, D. A. & Sabatini, D. M. Defining the role of mTOR in cancer. *Cancer Cell* **12**, 9–22 (2007).
56. Meric-Bernstam, F. & Gonzalez-Angulo, A. M. Targeting the mTOR signaling network for cancer therapy. *J. Clin. Oncol. Off. J. Am. Soc. Clin. Oncol.* **27**, 2278–2287 (2009).
57. Liu, P. *et al.* PtdIns(3,4,5)P3-Dependent Activation of the mTORC2 Kinase Complex. *Cancer Discov.* **5**, 1194–1209 (2015).
58. L, L., S, D., W, L. & Ca, P. mTORC2 regulates neutrophil chemotaxis in a cAMP- and RhoA-dependent fashion. *Dev. Cell* **19**, 845–857 (2010).

59. Shimokawa, H., Sunamura, S. & Satoh, K. RhoA/Rho-Kinase in the Cardiovascular System. *Circ. Res.* **118**, 352–366 (2016).

60. Sapoń, K., Mańka, R., Janas, T. & Janas, T. The role of lipid rafts in vesicle formation. *J. Cell Sci.* **136**, jcs260887 (2023).

61. Elsherbini, A. & Bieberich, E. Ceramide and exosomes: a novel target in cancer biology and therapy. *Adv. Cancer Res.* **140**, 121–154 (2018).

62. López-Montero, I. *et al.* Rapid Transbilayer Movement of Ceramides in Phospholipid Vesicles and inHumanErythrocytes *. *J. Biol. Chem.* **280**, 25811–25819 (2005).

63. Megha & London, E. Ceramide selectively displaces cholesterol from ordered lipid domains (rafts): implications for lipid raft structure and function. *J. Biol. Chem.* **279**, 9997–10004 (2004).

64. Sun, J. *et al.* CD24 blunts the sensitivity of retinoblastoma to vincristine by modulating autophagy. *Mol. Oncol.* **14**, 1740–1759 (2020).

65. Iqbal, M. S., Tsuyama, N., Obata, M. & Ishikawa, H. A novel signaling pathway associated with Lyn, PI 3-kinase and Akt supports the proliferation of myeloma cells. *Biochem. Biophys. Res. Commun.* **392**, 415–420 (2010).

66. Su, N. *et al.* Lyn is involved in CD24-induced ERK1/2 activation in colorectal cancer. *Mol. Cancer* **11**, 43 (2012).

67. Wimalachandra, D. *et al.* Long-chain glucosylceramides crosstalk with LYN mediates endometrial cell migration. *Biochim. Biophys. Acta BBA - Mol. Cell Biol. Lipids* **1863**, 71–80 (2018).

68. Sonnino, S. *et al.* Role of very long fatty acid-containing glycosphingolipids in membrane organization and cell signaling: the model of lactosylceramide in neutrophils. *Glycoconj. J.* **26**, 615–621 (2009).
69. Horbay, R. *et al.* Role of Ceramides and Lysosomes in Extracellular Vesicle Biogenesis, Cargo Sorting and Release. *Int. J. Mol. Sci.* **23**, 15317 (2022).
70. Kolesnick, R. The therapeutic potential of modulating the ceramide/sphingomyelin pathway. *J. Clin. Invest.* **110**, 3–8 (2002).
71. Stancevic, B. & Kolesnick, R. Ceramide-rich platforms in transmembrane signaling. *FEBS Lett.* **584**, 1728–1740 (2010).
72. Marchesini, N. & Hannun, Y. A. Acid and neutral sphingomyelinases: roles and mechanisms of regulation. *Biochem. Cell Biol.* **82**, 27–44 (2004).
73. Ira & Johnston, L. J. Sphingomyelinase generation of ceramide promotes clustering of nanoscale domains in supported bilayer membranes. *Biochim. Biophys. Acta BBA - Biomembr.* **1778**, 185–197 (2008).
74. Gómez-Muñoz, A. Modulation of cell signalling by ceramides. *Biochim. Biophys. Acta BBA - Lipids Lipid Metab.* **1391**, 92–109 (1998).
75. Gómez-Muñoz, A. Ceramide 1-phosphate/ceramide, a switch between life and death. *Biochim. Biophys. Acta BBA - Biomembr.* **1758**, 2049–2056 (2006).
76. Gómez-Muñoz, A. *et al.* Ceramide-1-phosphate promotes cell survival through activation of the phosphatidylinositol 3-kinase/protein kinase B pathway. *FEBS Lett.* **579**, 3744–3750 (2005).

77. Wang, H., Huang, H. & Ding, S.-F. Sphingosine-1-phosphate promotes the proliferation and attenuates apoptosis of Endothelial progenitor cells via S1PR1/S1PR3/PI3K/Akt pathway. *Cell Biol. Int.* **42**, 1492–1502 (2018).

78. Xiao, S., Peng, K., Li, C., Long, Y. & Yu, Q. The role of sphingosine-1-phosphate in autophagy and related disorders. *Cell Death Discov.* **9**, 1–14 (2023).

Figure legends

Figure 1. CD24 expression is associated with the PI3K-Akt signaling and mTOR pathways. (A) Hierarchical cluster analysis showing the clade of 44 genes (41 annotated) with similar differential gene expression patterns as *CD24a*. (B) Pathway network analysis generated from the differentially expressed 41-gene list identified the PI3K/Akt and mTOR signaling pathway as being associated with CD24 expression in developing B cells. The red boxes indicate nodes with terms related to PI3K-Akt or mTOR signaling. (C) WEHI-231-GFP cells were pre-treated with LY294002 or DMSO (vehicle control) for 15 min then cells were stimulated with isotype antibody or anti-CD24 stimulating antibody for the times indicated. PIP_3 levels were analyzed by ELISA, n=4, significance was determined by a one-way ANOVA followed by the Sidak's multiple comparison test *P<0.05.

Figure 2. CD24-mediated EV release is regulated by PI3K. (A-B) WEHI-231-GFP cells were pre-treated with LY294002 or DMSO for 15 min, then stimulated with anti-CD24 (CD24) or isotype control (isotype, iso) for 15 min, followed by washout and then a 24 h co-culture with WEHI-303-tdTomato cells. (A) Percent GFP and tdTomato double-positive cells and (B) Percent IgM and tdTomato double-positive cells after 24 h incubation. n=6, statistical significance determined by a two-way ANOVA (interaction significant at P=0.0003 for A and P=0.0002 for B) followed by the Sidak's multiple comparison test *P<0.05, ****P<0.001. C) Total cell lysates from WEHI-231-GFP cells pre-treated with DMSO or LY2940002 for 15 min, then stimulated with the above antibodies for different times indicated. Phosphorylated Akt and total Akt expression levels were determined by immunoblotting. D) WEHI-231-GFP cells were transfected with scrambled control siRNA or PI3K siRNA, and PI3K and GAPDH levels determined by immunoblotting. (E-F) WEHI-231-GFP cells with or without PI3K siRNA knock-down were stimulated with anti-CD24 or isotype for 15 min, followed by washout and then a 24 h co-culture with WEHI-303-tdTomato cells. (E) Percent GFP and tdTomato double-positive cells and (F) Percent IgM and tdTomato double-positive cells after 24 h incubation. n=3, statistical significance determined by a two-way ANOVA (interaction significant at P=0.0015 for E and P=0.0088 for F) followed by the Sidak's multiple comparison test **P<0.01, ***P<0.005.

Figure 3. CD24-mediated EV release is dependent on Akt and mTOR signaling pathways. (A-B) WEHI-231-GFP cells were pre-treated with MK-2206 or DMSO for 15 min, then stimulated with anti-CD24 or isotype control for 15 min, followed by washout and then a 24 h co-culture with WEHI-303-tdTomato cells. (A) Percent GFP and tdTomato double-positive cells and (B) Percent IgM and tdTomato double-positive cells after 24 h incubation. n=4, statistical significance determined by a two-way ANOVA (interaction significant at P=0.0074 for A and P=0.0002 for B) followed by the Sidak's multiple comparison test *P<0.05, **P<0.01, ****P<0.001. (C-D) WEHI-231-GFP cells were pre-treated with Torin 1 or Rapamycin or JR-AB2-011 or DMSO for 15 min, then stimulated with anti-CD24 or isotype control for 15 min, followed by washout and then a 24 h co-culture with WEHI-303-tdTomato cells. (C) Percent GFP and tdTomato double-positive cells and (D) Percent IgM and tdTomato double-positive cells after 24 h incubation. n=4, statistical significance determined by a two-way ANOVA (interaction significant at P=0.0143 for C and P=0.0066 for D) followed by the Sidak's multiple comparison test *P<0.05, **P<0.01, ***P<0.005, ****P<0.001.

Figure 4. CD24-mediated EV secretion is dependent on ROCK. (A-B) WEHI-231-GFP cells were pre-treated with Y27632 or DMSO for 15 min, then stimulated with anti-CD24 (CD24) or isotype control (isotype, iso) for 15 min, followed by washout and then a 24 h co-culture with WEHI-303-tdTomato cells. (A) Percent GFP and tdTomato double-positive cells and (B) Percent IgM and tdTomato double-positive cells after 24 h incubation. n=6, statistical significance determined by a two-way ANOVA (interaction significant at P=0.03 for A and P=0.0069 for B) followed by the Sidak's multiple comparison test *P<0.05, **P<0.01, ***P<0.005, ****P<0.001. C) Total cell lysates from WEHI-231-GFP cells pre-treated with DMSO or Y27632 for 15 min, then stimulated with the above antibodies for different times indicated. Phosphorylated Cofilin and total Cofilin expression levels were determined by immunoblotting. D) WEHI-231-GFP cells were transfected with scrambled control siRNA or ROCK siRNA, and ROCK and GAPDH levels determined by immunoblotting. (E-F) WEHI-231-GFP cells with or without ROCK siRNA knock-down were stimulated with anti-CD24 or isotype for 15 min, followed by washout and then a 24 h co-culture with WEHI-303-tdTomato cells. (E) Percent GFP and tdTomato double-positive cells and (F) Percent IgM and tdTomato double-positive cells after 24 h incubation. n=3, statistical significance determined by a two-way ANOVA (interaction

significant at P=0.0011 for E and P=0.0013 for F) followed by the Sidak's multiple comparison test ***P<0.005, ****P<0.001.

Figure 5. CD24-mediated EV release is controlled by actin cytoskeleton re-organization and aSMase activity. (A-B) WEHI-231-GFP cells were pre-treated with Cytochalasin D or DMSO for 15 min, then stimulated with anti-CD24 or isotype control for 15 min, followed by washout and then a 24 h co-culture with WEHI-303-tdTomato cells. (A) Percent GFP and tdTomato double-positive cells and (B) Percent IgM and tdTomato double-positive cells after 24 h incubation. n=4, statistical significance determined by a two-way ANOVA (interaction significant at P=0.0017 for A and P=0.0027 for B) followed by the Sidak's multiple comparison test **P<0.01, ***P<0.005, ****P<0.001. (C-D) WEHI-231-GFP cells were pre-treated with Imipramine or DMSO for 15 min, then stimulated with anti-CD24 or isotype control for 15 min, followed by washout and then a 24 h co-culture with WEHI-303-tdTomato cells. (C) Percent GFP and tdTomato double-positive cells and (D) Percent IgM and tdTomato double-positive cells after 24 h incubation. n=4, statistical significance determined by a two-way ANOVA (interaction significant at P=0.0006 for C and P=0.0006 for D) followed by the Sidak's multiple comparison test ***P<0.005, ****P<0.001. (E) WEHI-231-GFP cells were pre-treated with imipramine or DMSO (vehicle control) for 15 min then cells were stimulated with isotype antibody or anti-CD24 stimulating antibody for the times indicated. PIP_3 levels were analyzed by ELISA, n=5, significance was determined by a one-way ANOVA followed by the Sidak's multiple comparison test *P<0.05, **P<0.01.

Figure 6. Inhibition of PI3K, ROCK, and aSMase is not additive. WEHI-231-GFP cells were pre-treated with LY294002 or Y27632 or Imipramine or inhibitor combinations or DMSO for 15 min, then stimulated with anti-CD24 or isotype control for 15 min, followed by washout and then a 24 h co-culture with WEHI-303-tdTomato cells. (A) Percent GFP and tdTomato double-positive cells and (B) Percent IgM and tdTomato double-positive cells after 24 h incubation respectively, are shown. n=4, statistical significance determined by a two-way ANOVA (interaction significant at P<0.0001 for A and P=0.0008 for B) followed by the Sidak's multiple comparison test **P<0.01, ***P<0.005, ****P<0.001.

Figure 7. Representative images of WEHI-231-GFP cells show EV release and cell activation. WEHI-231-GFP cells were pre-treated with LY294002 or Y27632 or DMSO for 15 min, then stimulated with anti-CD24 or isotype control. (A) The cells were captured at 15 min after stimulation. White arrows indicate EV release. Scale bar = 2 mm. The analysis of cell activation was observed and marked at 3 levels of activation by 4 different indiviuals who were blinded to the treatments. Cell activation was determined at B) 15 min and C) 30 min after stimulation. n=4, statistical significance determined by a two-way ANOVA (interaction significant at P<0.0001 for B and P<0.0001 for C) followed by the Sidak's multiple comparison test *P<0.05, ***P<0.005.

Supplemental Figure S1. Pre-treatment with inhibitor on donor WEHI-231-GFP cells inhibits the transfer of GFP and IgM from donor to recipient cells in response to CD24. (A) The percentage of cells positive for GFP and tdTomato. (B) WEHI-231-GFP are 100% IgM positive while WEHI-303-tdTomato cells do not express IgM on their cell membrane. (C) Schematic of experimental design of model system. WEHI-231-GFP cells were pre-treated with a chemical, for example, LY294002 or DMSO, for 15 min, then stimulated with isotype control or anti-CD24 for 15 min, followed by washout and then a 24 h co-culture with WEHI-303-tdTomato cells. Representative dotplots of GFP-positive (D) and IgM-positive (E) on WEHI-303-tdTomato cells after co-culture with stimulated donor WEHI-231-GFP cells.

Supplemental Figure S2. Neither nSMase nor calcium regulates EV release. (A-B) WEHI-231-GFP cells were pre-treated with GW4869 or DMSO for 15 min, then stimulated with anti-CD24 or isotype control for 15 min, followed by washout and then a 24 h co-culture with WEHI-303-tdTomato cells. (A) Percent GFP and tdTomato double-positive cells and (B) Percent IgM and tdTomato double-positive cells after 24 h incubation. n=4, statistical significance determined by a two-way ANOVA (interaction significant at P=0.2669 for A and P=0.4195 for B) followed by the Sidak's multiple comparison test ***P<0.005, ****P<0.001. (C-D) WEHI-231-GFP cells were stimulated with isotype control, anti-CD24, ionomycin or ionomycin removed after 15 min, followed by 24 h co-culture with WEHI-303-tdTomato cells. (C) Percent GFP and tdTomato double-positive cells. (D) Percent IgM and tdTomato double-positive cells after 24 h incubation.

n=4, statistical significance was determined by a one-way ANOVA followed by the Sidak's multiple comparison test ****P<0.001.

Supplemental Files 1-8. Videos of cell activation in response to CD24 after 15 min or 30 min in the presence or absence of LY294002 or Y27632.

Graphical abstract

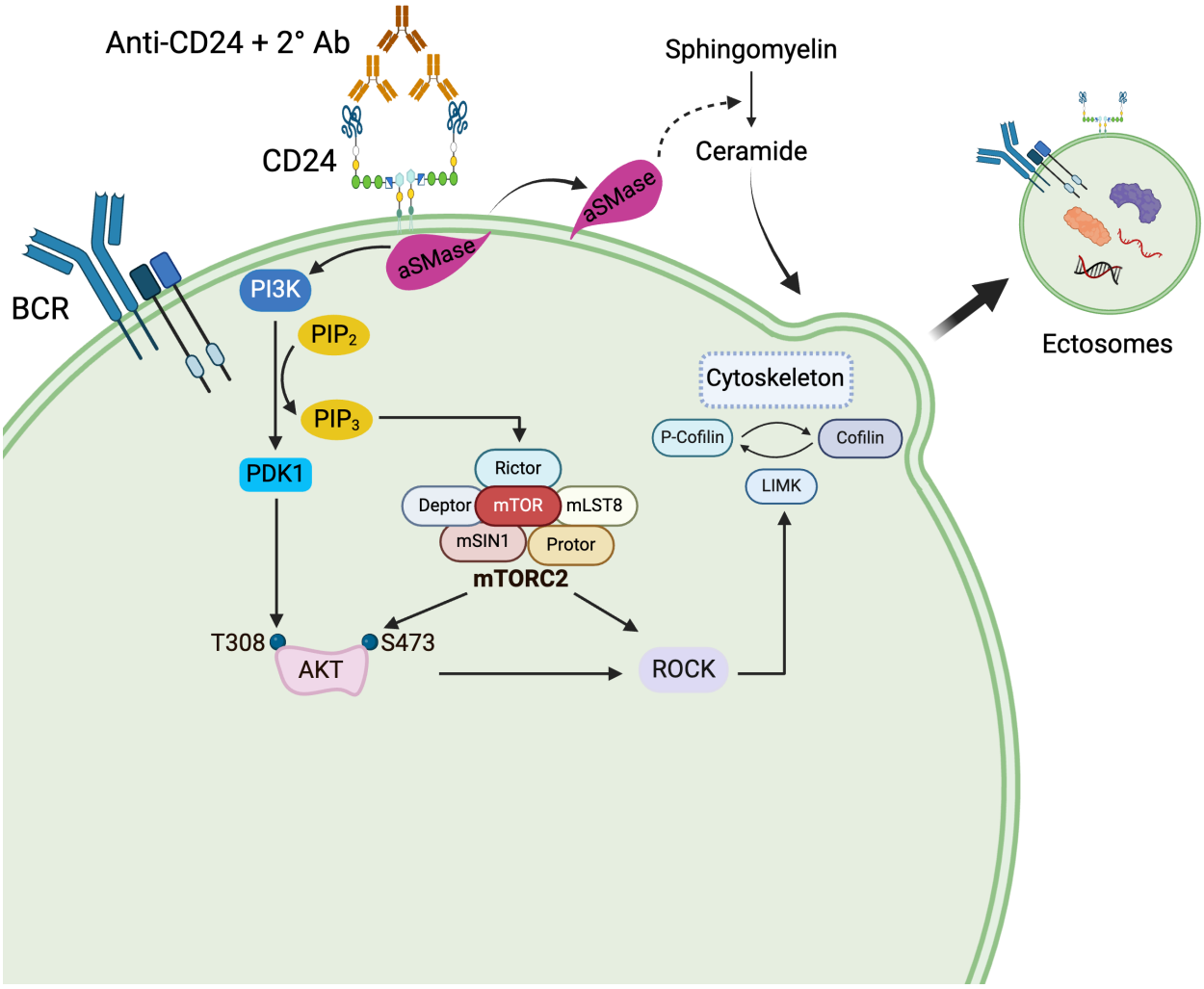

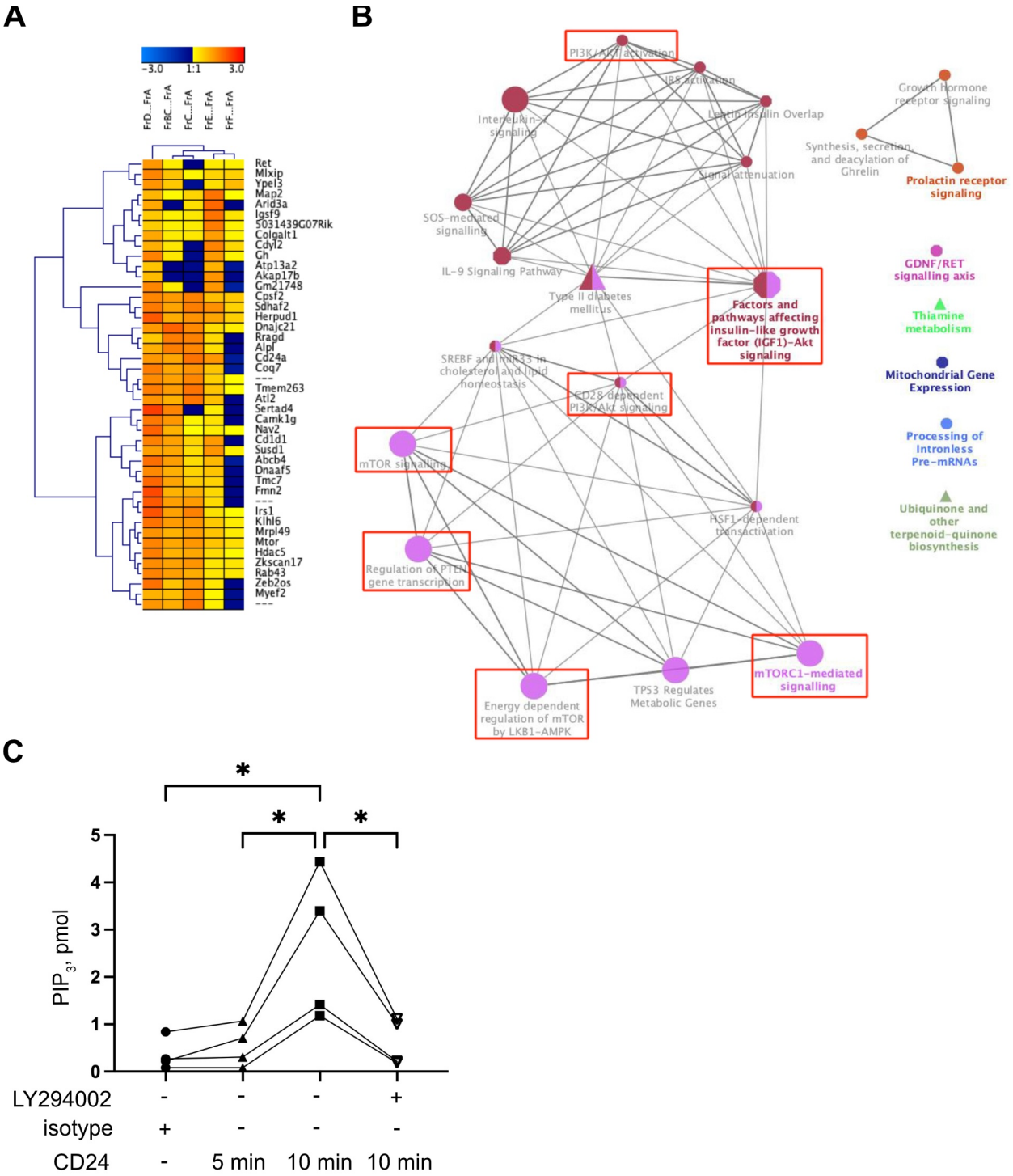

Figure 1. CD24 expression is associated with the PI3K-Akt signaling and mTOR pathways.

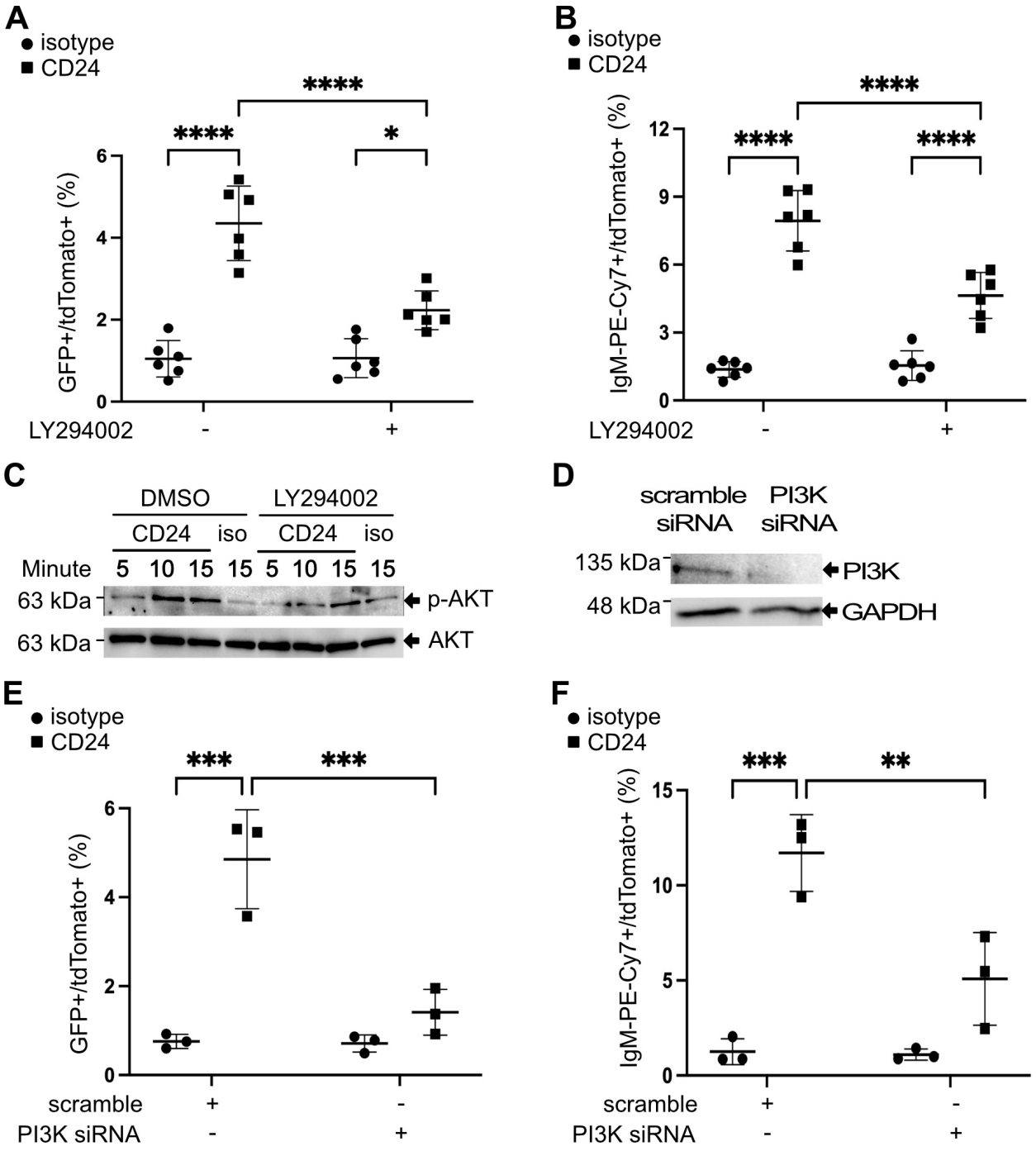

Figure 2. CD24-mediated EV release is regulated by PI3K.

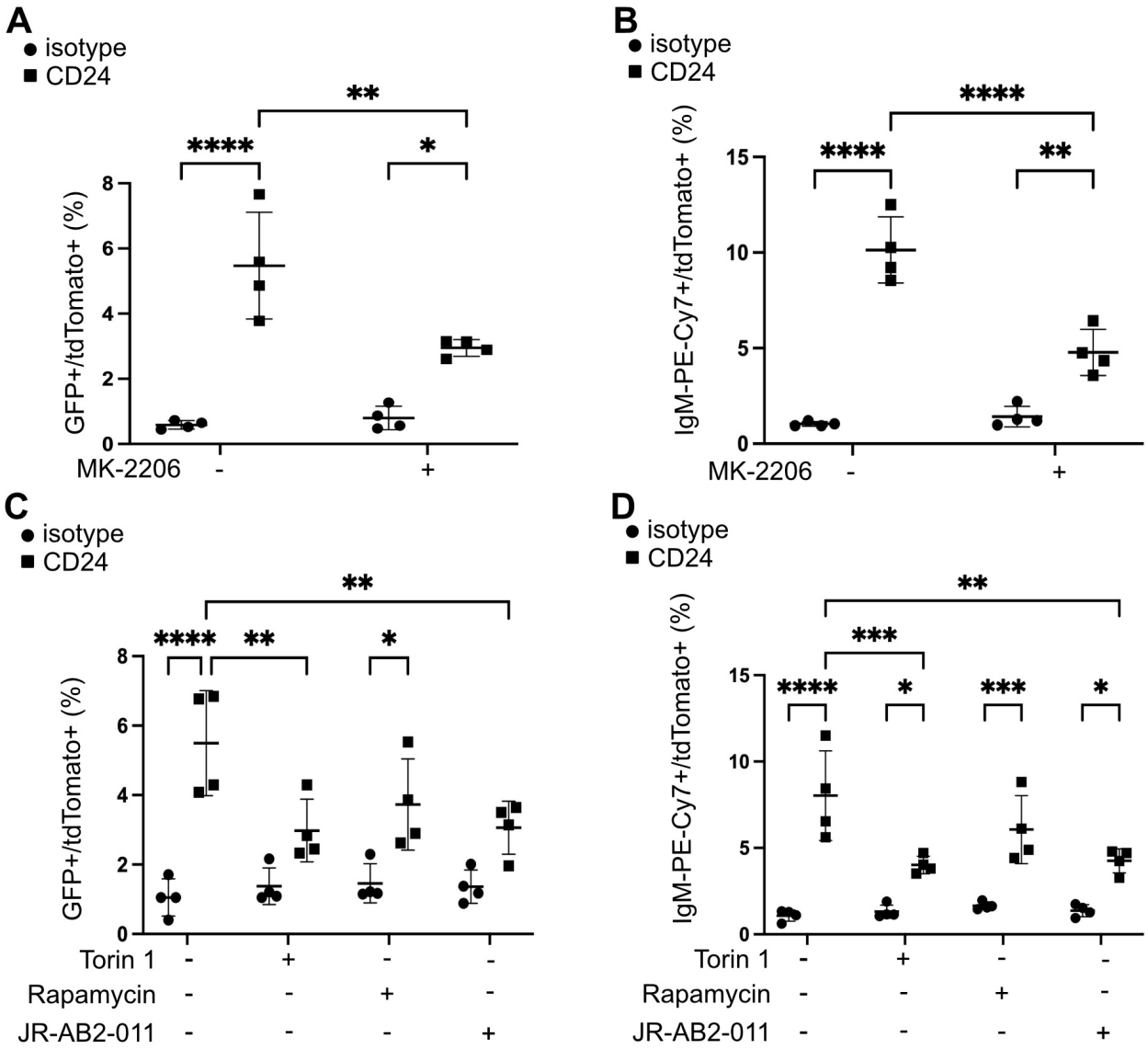

Figure 3. CD24-mediated EV release is dependent on Akt and mTOR signaling pathways.

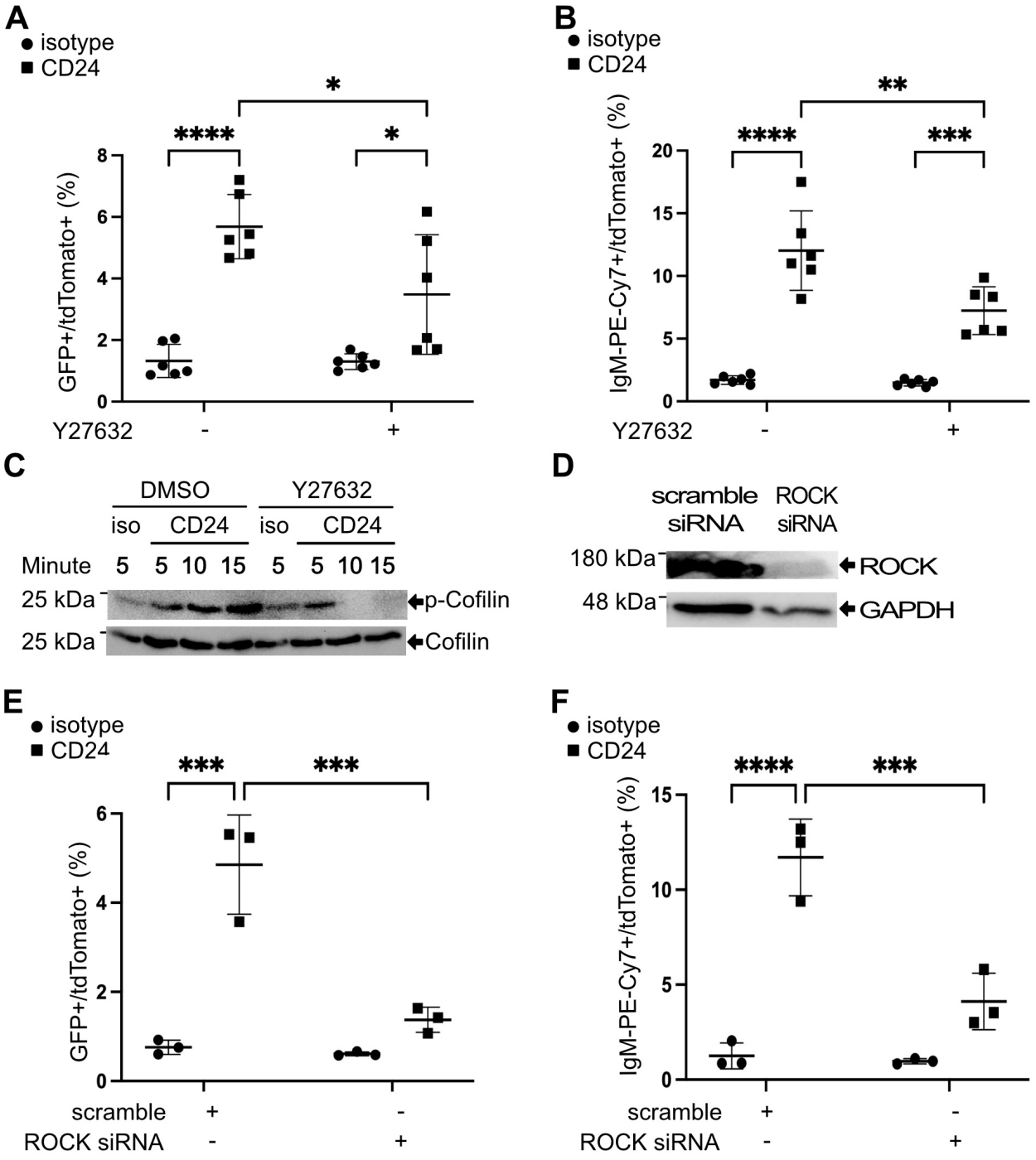

Figure 4. CD24-mediated EV secretion is dependent on ROCK.

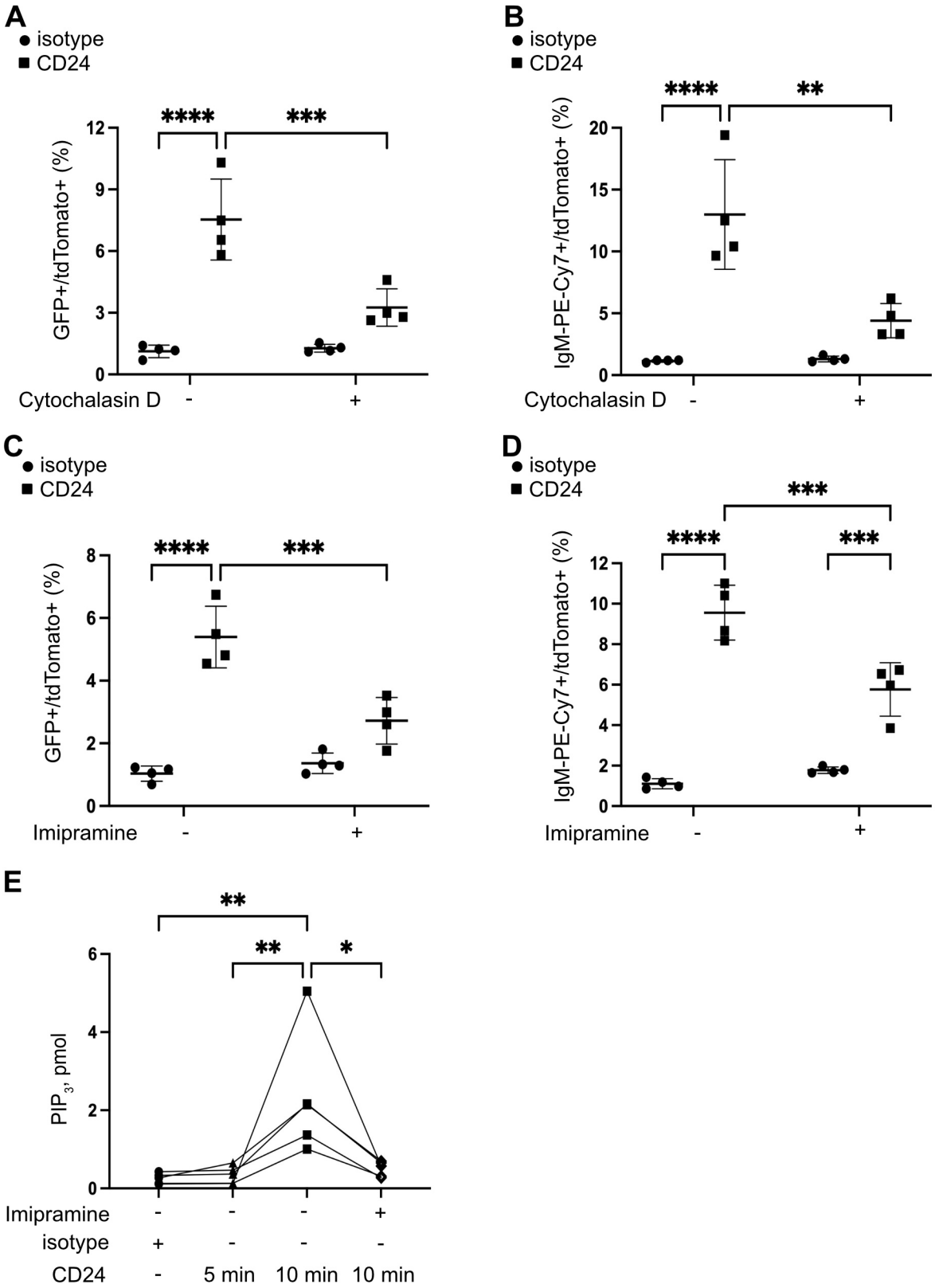

Figure 5. CD24-mediated EV release is controlled by actin cytoskeleton re-organization and aSMase activity.

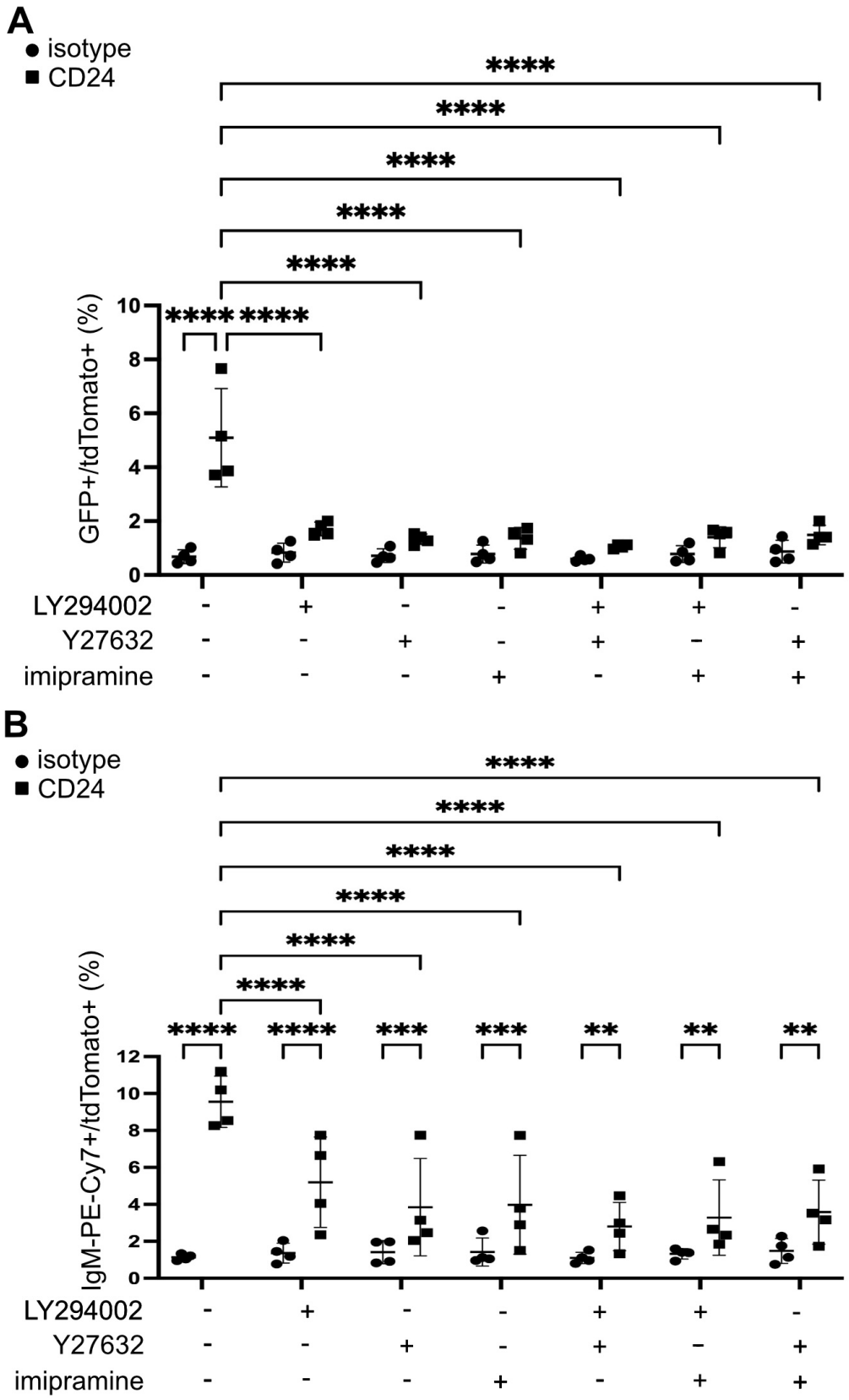

Figure 6. Inhibition of PI3K, ROCK, and aSMase is not additive.

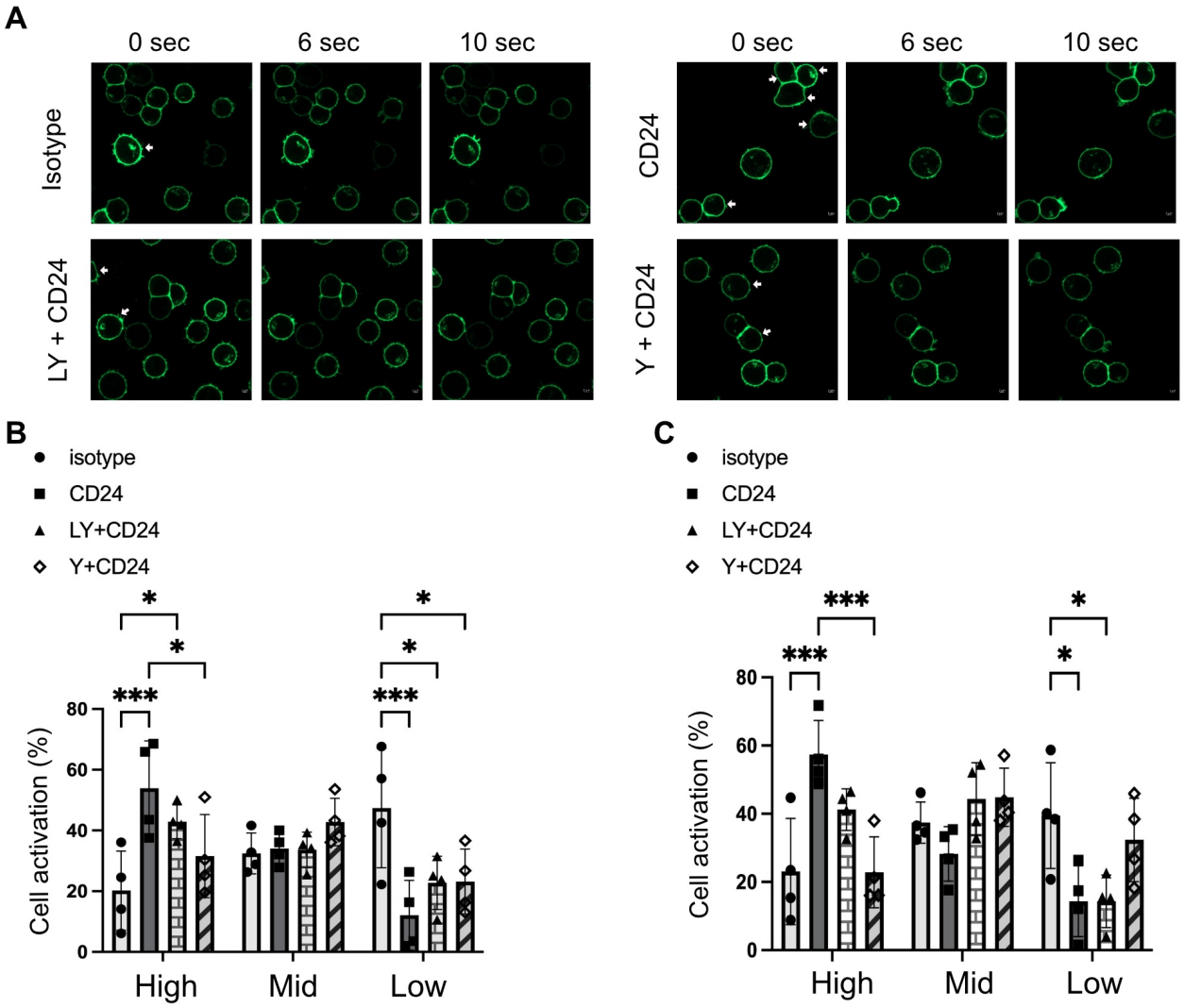

Figure 7. Representative images of WEHI-231-GFP cells show EV release and cell activation.